Modeling the Yule–Nielsen Halftone Effect

J. S. Arney* and Charles D. Arney

Chester F. Carlson Center for Imaging Science, Rochester Institute of Technology, Rochester, New York

P. G. Engeldrum*

Imcotek, Inc., Winchester, Massachusetts

The Yule–Nielsen effect, also called optical dot gain, is a nonlinear relationship between the reflectance of a halftone image and the fractional dot area of the halftone dots. Two models of the Yule–Nielsen effect are examined. The first is an empirical model previously described in the literature, and the second is an a priori model derived for an idealized halftone line system in one spatial dimension. Both are shown to model halftone behavior well. By combining the two models we derive a semiempirical function that establishes a simple connection between the magnitude of the Yule–Nielsen effect and independently measurable scattering characteristics of the paper. The potential utility of this semiempirical model for characterizing the impact of other factors, such as the shape of halftone dots and depth of ink penetration, is discussed.

Journal of Imaging Science and Technology 40:3 233–238(1996)

Introduction

Dot gain, a concept long associated with halftone imaging, refers to the generally observed phenomenon that a printed dot pattern appears darker than one would expect on the basis of the nominal size of the dot intended by the printing process. Physical reasons for dot gain are many, including the lateral spread of ink during transfer from a lithographic plate and the lateral diffusion of inkjet drops as they strike the paper. Once the image has been printed, the actual dot area may be measured. Conservation of photon energy suggests the Murray–Davies equation,[1]

$$R(F_i) = F_i R_i + (1 - F_i)R_p. \quad (1)$$

In this equation the macroscopic reflectance, $R(F_i)$, is linearly scaled between the reflectance of the paper, R_p, and the reflectance of the ink, R_i, with the fractional dot area $0 \le F_i \le 1$. For example, if one were to print a halftone dot of area fraction $F_i = 0.5$, and if the respective paper and ink reflectances were 1.00 and 0.00, then one would expect a macroscopic reflectance of $R = 0.50$. However, an experimental measurement almost always results in a reflectance significantly less than that predicted by the Murray–Davies equation. This effect, which is different from physical dot gain, is called the *Yule–Nielsen effect*, or *optical dot gain*.[2]

During the past several decades the nonlinear relationship observed between R and F_i,

$$R(F_i) = [F_i R_i^{1/n} + (1 - F_i)R_p^{1/n}]^n, \quad (2)$$

has been modeled empirically and quite successfully with Eq. 2, the Yule–Nielsen equation.[3,4] Experimentally one may adjust the value of n to achieve the best fit between Eq. 2 and measured values of R and F_i. The Yule–Nielsen equation generally provides an excellent fit to experimental data with values of n typically falling in the range $1 \le n \le 2$.[5] However, it would also be useful to be able to predict the n value based on underlying paper and ink optical parameters. Both theoretical and empirical attempts have been made to relate the Yule–Nielsen n value to the fundamental physical and optical parameters of ink and paper,[6–12] but these have largely fallen short of providing practical solutions to the problem.[13] Part of the difficulty in relating n to fundamental parameters may be a reflection of the fact that the Yule–Nielsen equation, though a useful and often accurate model of tone reproduction, is intrinsically incorrect. Photon flux, and thus reflectance, should add linearly, as suggested by the Murray–Davies (Eq. 1), rather than by the power factor of $1/n$ in Eq. 2. The objective of the current project has been to replace the Yule–Nielsen model with models that can more easily be related to fundamental physical and optical parameters of the system. As will be shown, the magnitude of the Yule–Nielsen effect can be predicted quantitatively from the measured scattering characteristics of papers.

An Empirical Alternative to Yule–Nielsen

The underlying cause of the nonlinearity between R and F_i, as suggested by Yule and Nielsen in their original work,[3,11] is that light that strikes the paper between halftone dots does not always reflect back from the point at which it entered the paper. Rather, light scatters and often emerges under a halftone dot and is thus absorbed. Thus the overall reflectance of the image is lower than would be expected in the absence of lateral scattering. In addition, recent reports of microdensitometric analysis of halftones has shown that both the reflectance of the paper between the dots, R_p, and the reflectance of the halftone dot, R_i, decrease as the dot area fraction, F_i, increases.[7,14,15] The data in Fig. 1 illustrate a typical case for the mean reflectance values of ink dots and of paper between the dots, measured by microdensitometry as described in the Appendix.

Original manuscript received November 4, 1995.

* IS&T Member

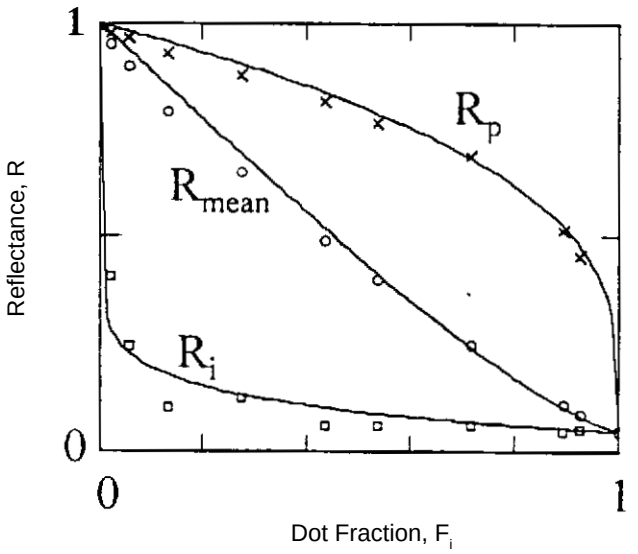

Figure 1. Reflectance values for a 65 lpi (2.6 cycles/mm) halftone gray scale printed with a wax thermal transfer printer. Values R, R_i, and R_p are, respective reflectance values for the overall image, the halftone dots, and the paper between the dots, measured as described in the Appendix. Solid lines are modeled with empirical constants w = 0.35 and v = 0.05.

As shown before,[15] the changes in R_i and R_p with F_i observed in experiments such as that shown in Fig. 1 can be modeled empirically by Eqs. 3 and 4.

$$R_i(F_i) = R_g[1-(1-T_i)F_i^w]\cdot[1-(1-T_i)F_i^v]. \quad (3)$$

$$R_p(F_p) = R_g[1-(1-T_i)(1-F_p^w)]\cdot[1-(1-T_i)(1-F_p^v)]. \quad (4)$$

In these equations $F_p = 1 - F_i$, and R_g is the reflectance of the unprinted paper; T_i is the transmittance of the ink at 100% dot. Assuming Beer–Lambert transmission, $T_i = (R_{ink}/R_g)^{1/2}$, where R_{ink} is the reflectance of the ink image at 100% dot. The power factors, w and v, are identical in both equations and are adjusted empirically to achieve a good fit between the equations and the measured values of paper and ink reflectances at each value of F_i. The resulting reflectance values are then used in the Murray–Davies equation [Eq. 1 with $R_p = R_p(F_p)$ and $R_i = R_i(F_i)$] to calculate the overall R versus F_i. This empirical model has been shown to model the Yule–Nielsen effect as well as the Yule–Nielsen equation.[15] The solid lines drawn thorough the data in Fig. 1 were modeled in this way.

The empirical w,v model was observed to fit as well as, but not better than, the much simpler Yule–Nielsen model when applied to a variety of halftone types produced with a variety of impact and non-impact printing technologies.[15] However, it was suggested that the w,v model may offer a better connection with the fundamental physical and optical parameters of the system. In particular, the w factor may be related to the lateral scattering power of the paper and the v factor to the lateral distribution of ink at the edge of the dot. As described below, these relationships can be established theoretically, and combining the theoretical analysis with the empirical w,v model leads to derivation of a semiempirical relationship that directly and simply relates the magnitude of the Yule–Nielsen effect to independently measurable parameters of the system. Moreover, the results suggest an experimental means for quantitatively characterizing the impact of other factors, such as the shapes of halftone dots or the extent of penetration of ink-jet ink, on the Yule–Nielsen effect.

An a priori Model of an Ideal Halftone

A simple, one-dimensional halftone system is one with lines rather than dots, and we assume ink having Beer–Lambert transmittance. The ink is also assumed to rest on top of the paper substrate with no penetration into the paper. The Fourier series of Eq. 5 provides the basis for a description of this idealized halftone system:

$$f_i(x) = F_p + \frac{2}{\pi}\sum_{n=1}^{\infty}\frac{-1^n}{n}\sin(n\pi F_p)\cos(2\pi n\omega_o x). \quad (5)$$

The paper fraction is $F_p = 1 - F_i$, and ω_o is the line frequency of the halftone. These and other terms are described in Fig. 2. We can scale this function to describe the transmittance pattern of the halftone lines:

$$T_i(x) = f_i(x)(1-T_i)+T_i. \quad (6)$$

If the edge of the halftone line is not perfectly sharp, we can modify the Fourier series as shown in Eq. 7. The MTF_i function in this equation,

$$f_i(x) = F_p + \frac{2}{\pi}\sum_{n=1}^{\infty}\frac{-1^n}{n}\sin(n\pi F_p)\cos(2\pi n\omega_o x)MTF_i(n\omega_o), \quad (7)$$

is a Fourier description of the lateral distribution of colorant at the edge of the dot. If the dot has a perfectly sharp edge, then $MTF_i = 1$ and Eq. 7 is the same as Eq. 5.

Applying Eq. 7 to Eq. 6 not only describes the transmittance pattern of the halftone dots; it also describes the irradiance of light entering the paper after passing the halftone dots. After this pattern of light enters the paper it is scattered and some is absorbed. Scattering is described with an MTF_p function as shown in Eq. 8.

$$f_p(x) = F_p + \frac{2}{\pi}\sum_{n=1}^{\infty}\frac{-1^n}{n}\sin(n\pi F_p)\cos(2\pi n\omega_o x) \cdot MTF_i(n\omega_o)MTF_p(n\omega_o). \quad (8)$$

Absorption of light is governed by the reflectance factor of the paper, R_g. With R_g and the series expression of Eq. 8 one can model the overall irradiance pattern reflected from the paper with Eq. 9:

$$I_r(x) = R_g[f_p(x)(1-T_i)+T_i]. \quad (9)$$

This pattern of light then encounters the transmittance pattern of the halftone dots to produce a final reflected pattern, $R(x)$, given by Eq. 10.

$$R(x) = I_r(x)\cdot T_i(x). \quad (10)$$

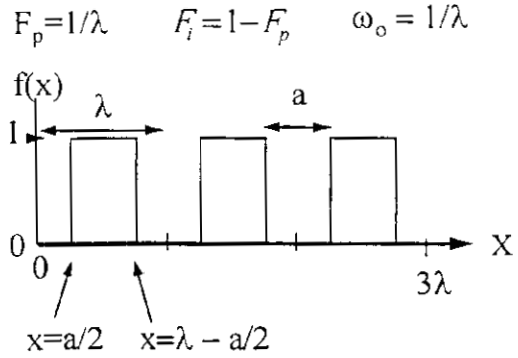

Figure 2. Diagram of the Fourier series of Eq. 5.

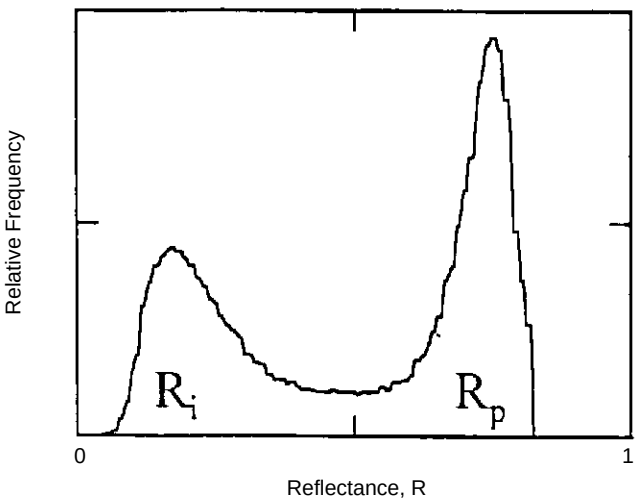

Figure 3. Histogram showing the relative frequency of occurrence of reflectance values in halftone images captured at 40× magnification. R_i and R_p are reflectance values at the peaks respectively corresponding to ink dots and to paper between the dots.

Relating Theory to Data

If we set $x = \lambda/2$ in Fig. 2 and in Eq. 10, then we have the reflectance $R(\lambda/2)$ for the paper at the point equidistant between two halftone lines. Similarly, if we set $x = 0$ in Eq. 10 we have the reflectance $R(0)$ for the center of the halftone line. These quantities can be measured experimentally with the image microdensitometer described in the Appendix. However, it is easier experimentally and more precise statistically to examine the histogram of reflectance values captured over a 4-mm field of view of a halftone dot pattern. Figure 3 shows such a histogram for a halftone pattern printed at a nominal 50% dot area by offset lithography. The average reflectance of the paper between the halftone lines is located at the right-hand peak of the histogram. Similarly, the average reflectance of the halftone line is indicated by the peak on the left side of the histogram. These mean value reflectances can be modeled by integrating Eq. 10 from $x = (a/2)$ to $x = \lambda - (a/2)$. Similarly, the mean value of the reflectance of the ink dot can be modeled by integrating from $x = -a/2$ to $x = +a/2$. With some algebraic manipulation this leads to the following expressions for R_p and R_i:

$$R_p(F_p) = R_g[G_p(F_p)(1-T_i)] + T_i]\cdot[G_i(F_p)(1-T_i)] + T_i], \quad (11)$$

$$R_i(F_i) = R_g[H_p(F_i)(1-T_i)] + T_i]\cdot[H_i(F_i)(1-T_i)] + T_i], \quad (12)$$

where we have the following series expressions resulting from the integration:

$$G_p(F_p) = F_p \sum_{n=-\infty}^{\infty} \mathrm{sinc}^2(nF_p)\mathrm{MTF}_i(n\omega_o)\mathrm{MTF}_p(n\omega_o), \quad (13)$$

$$G_i(F_p) = F_p \sum_{n=-\infty}^{\infty} \frac{-1^n}{n}\mathrm{sinc}^2(nF_p)\mathrm{MTF}_i(n\omega_o), \quad (14)$$

$$H_p(F_i) = 1 - F_i \sum_{n=-\infty}^{\infty} \mathrm{sinc}^2(nF_i)\mathrm{MTF}_i(n\omega_o)\mathrm{MTF}_p(n\omega_o), \quad (15)$$

$$H_i(F_i) = 1 - F_i \sum_{n=-\infty}^{\infty} \mathrm{sinc}^2(nF_i)\mathrm{MTF}_i(n\omega_o). \quad (16)$$

The model represented by Eqs. 11 through 16 contains three independently measurable constants: R_g = reflectance of the unprinted paper; T_i = transmittance of the ink at $F_i = 1$; and ω_o = frequency of the halftone lines. Only two other items are required to calculate $R_i(F_i)$ and $R_p(F_i)$, and with Eq. 1 to calculate the overall, macroscopic reflectance of the halftone image. These two items are the MTF functions for the scatter of light in paper and the lateral spread of the ink edges.

In a recent MTF analysis of paper, it was shown that the lateral scattering of light in paper could be modeled closely with the following MTF function[16]:

$$MTF_p(\omega) = \frac{1}{1+(k_p\omega)^{1.7}}. \quad (17)$$

Values of the MTF constant, k_p, can be measured experimentally, either by analysis of Kubelka–Munk scattering and absorption coefficients[16–18] or by image analysis of various patterns of light projected onto the surface of the paper.[3,11,16,19,20] Because no MTF function that describes the softness of printed dot edges has been explored or reported in the literature, the following function was chosen arbitrarily:

$$MTF_i(\omega) = \frac{1}{1+(k_i\omega)^{1.7}}. \quad (18)$$

Although the a priori model appears complex, it is easily applied. Starting with four independently measurable constants, R_g, T_i, ω_o, and k_p, and one arbitrary constant, k_i, one can use sequentially Eqs. 18 back through 11 to calculate paper and ink reflectances as a function of F_i. Then Eq. 1 can be used to calculate the overall macroscopic reflectance.

An Experimental Test of the a priori Model

One-dimensional halftone gray scales were printed with offset lithography as described in the Appendix. The halftones ranged from 0 to 100% dot (F_i from 0 to 1) and were printed at 60 lpi (ω_o = 2.4 cycles/mm) on three different papers, called A, B, and C, with MTF_p constants k_p = 0.263, 0.455, and 2.00 mm, respectively, measured as described previously.[16] Paper A was a coated sheet, B was noncoated, and C was a resin-filled translucent sheet manufactured as a tracing paper. Paper B was also printed at 195 lpi (ω_o = 7.7 cycles/mm). The MTF constant of each paper had been characterized previously.[16] Mean values of paper and ink reflectance in the halftones were measured from reflectance histograms, as described in the Appendix. The print densities varied somewhat from paper to paper and from print run to print run. Thus, in order to compare results, relative reflectance values were calculated by linearly scaling reflectance over the range between 0 and 1 corresponding to relative reflectance of the ink at $F_i = 1.0$ and of the paper at $F_i = 0$. Figures 4 and 5 show the results.[21]

To model the lines in Figs. 4 and 5, values of R_g, T_i, and the MTF_p constants for Papers A, B, and C were used as measured and were not adjusted to minimize the difference between the data and the model. A value of k_i = 0.05 mm was chosen to provide the best fit to the data for Paper B at 7.7 cycles/mm. The same value then was used in all of the other models in Figs. 4 and 5.

Print quality in the lithographic print series was not very good, and there is much experimental noise in the microreflectance data. However, the significance of the model can still be seen in the trends. Figure 4 shows the experimental effect of changing the frequency, ω_o, of the

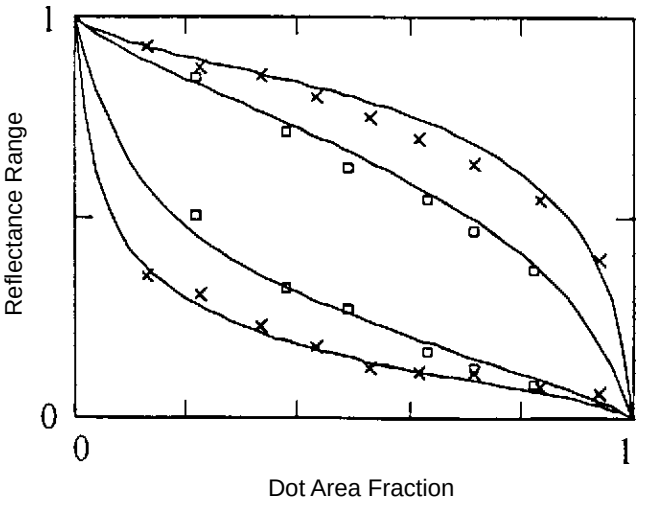

Figure 4. Reflectance range versus F_i for Paper B printed at ω_0= 2.4 cycles/mm (x) and at ω_0 = 7.7 cycles/mm (□). Both ink reflectance, R_i, and reflectance of the paper are between the dots, R_i, shown. Solid lines are modeled as described in the text.

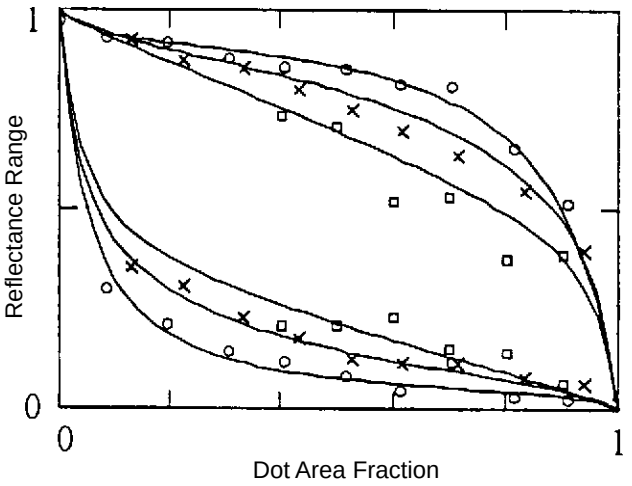

Figure 5. Reflectance range versus F_i for Papers A, B, and C (○, x, and □) with k_p = 0.263, 0.455, and 2.00 mm, respectively. The halftones are printed at 2.4 cycles/mm. Solid lines are modeled as described in the text.

halftone pattern. Figure 5 shows the effect of changing paper type, k_p. In both cases the experimental trends are closely modeled, as shown by the solid lines in the figures, by changing only the corresponding parameters, ω_o and k_p of the model, leaving the other parameters unchanged.

Combining the Empirical and a priori Models

The a priori model represented by Eqs. 11 through 18 relate the tone reproduction characteristics of halftone images and independently measurable parameters of the system. However, the model strictly applies only to an ideal, one-dimensional halftone with ink perfectly on top of the paper. The empirical model of Eqs. 3 and 4, on the other hand, has been shown to be generally applicable to a wide variety of halftone types produced by a wide variety of printing technologies.[15] If the empirical model is a close approximation of the behavior of real halftones, then we should be able to relate the w and v parameters of the empirical model to the independently measurable parameters of the a priori model. We can do this by equating Eqs. 3 and 11:

$$[1-(1-T_i)F_i^w]\cdot[1-(1-T_i)F_i^v] = [G_p(F_p)(1-T_i)]+T_i]\cdot[G_i(F_p)(1-T_i)]+T_i]. \quad (19)$$

Because the left side of Eq. 19 is empirically derived, we are free to relate the terms in brackets as follows:

$$[1-(1-T_i)F_i^w] = [G_p(F_p)(1-T_i)+T_i], \quad (20)$$

$$[1-(1-T_i)F_i^v] = [G_i(F_p)(1-T_i)+T_i]. \quad (21)$$

With algebraic manipulation we have the following:

$$w = \frac{\ln(G_p(F_p))}{\ln(F_p)}, \quad (22)$$

$$v = \frac{\ln(G_i(F_p))}{\ln(F_p)}. \quad (23)$$

The right side of Eq. 23 is a function only of F_p, k_i, and ω_o. Thus, as suggested originally, the power factor v depends on the edge sharpness, k_i, of the halftone dot. The right side of Eq. 22 contains the product $MTF_i \cdot MTF_p$ and thus is a function of both the edge sharpness, k_i, and the lateral scatter of light, k_p. However, in most cases observed in this laboratory the mean scattering distance of light is much greater than the dimensions of dot edges so that $k_p >> k_i$. When this is true, we can approximate the MTF of paper as $MTF_i \cdot MTF_p \approx MTF_p$. In this case the w power factor depends on the paper MTF constant, k_p, as suggested previously.[15]

In the empirical model the w and v factors are used as constants. However, Eqs. 22 and 23 imply that w and v are functions of the dot area fraction, F_i. To examine the severity of this deficiency in the w,v model, one can compare R_p versus F_i calculated with both Eqs. 4 and 11. This is done by selecting values of R_g, T_i, F_i, k_p, k_i, and ω_o and applying Eq. 11 to calculate R_p versus F_i. Then corresponding values of w and v are calculated from Eqs. 22 and 23 with $F_i = F_p = 0.5$, and these w and v values are used in Eq. 4 to calculate R_p versus F_i. Figure 6 is a typical example, and it is evident that, whereas the w,v model is not in exact agreement with the a priori model, the differences are very small.

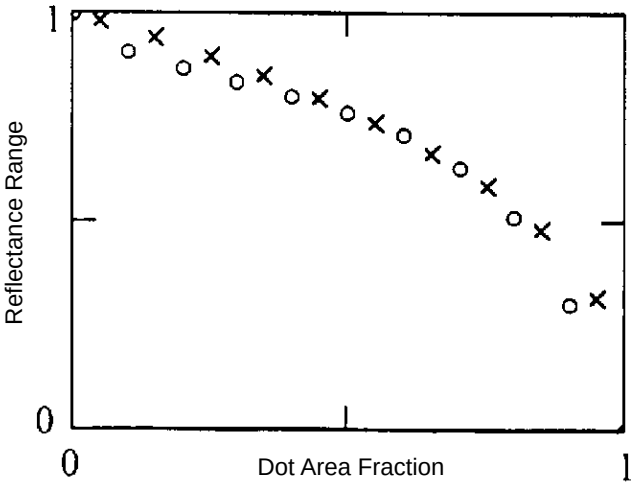

Figure 6. Reflectance of paper between halftone dots modeled (○) with Eq. 11 with k_p = 0.25 mm and k_i = 0.05 mm, and modeled (x) empirically with Eq. 4 using w = 0.332 and v = 0.056, as calculated from Eqs. 22 and 23 at F_i = 0.5.

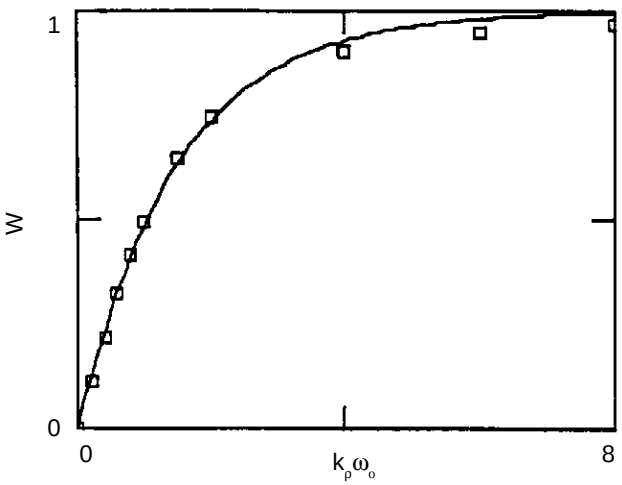

Figure 7. Points (□) are the empirical power factor, w, as a function of the product $k_p\omega_o$ calculated using Eq. 22 with $F_i = 0.5$. The line is Eq. 24 with A = 0.66.

If we select $F_i = F_p = 0.5$ in Eq. 22 we can calculate the relationship between w and k_p as shown in Fig. 7. The points in Fig. 7 were calculated with Eq. 22. However, the solid line is an empirical function fit to these calculated points with

$$w = 1 - e^{-Ak_p\omega}, \tag{24}$$

a simple exponential equation containing an empirical constant, A = 0.66. This empirical function is easier to use than Eq. 22 with the cumbersome series expression $G_p(F_p)$. To check the validity of Eq. 24 experimentally, a set of one-dimensional halftone patterns was printed by offset lithography at a series of line frequencies, ω_o, ranging from 2.4 to 7.7 cycles/mm on a series of papers measured previously, having values of k_p ranging from 0.09 to 1.60 mm.[15] Each paper was printed with a halftone gray scale with a dot fraction ranging $0.0 \le F_i \le 1.0$. For each paper at each frequency the product, $k_p\omega_o$, was noted. Then the empirical halftone model was fit to each gray scale, and the best fit value of the power constant, w, was plotted versus the product, $k_p\omega_o$. The results shown in Fig. 8 confirm that Eq. 24 adequately represents the behavior of one-dimensional halftones.

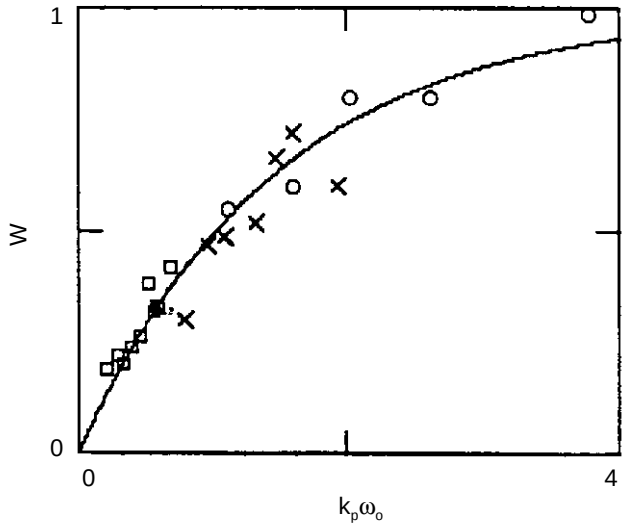

Figure 8. Power factor w as a function of the product $k_p\omega_o$ measured experimentally and modeled with Eq. 24. Points (□) are for a coated paper at k_p = 0.09 mm and ω_o from 2.4 to 7.7 cycles/mm. Points (x) are for a coated paper at k_p = 0.253 mm and ω_o from 2.4 to 7.7 cycles/mm. Points (○) are for a single halftone frequency of ω_o = 2.4 cycles/mm and a series of papers ranging from k_p = 0.253 to 1.6 mm.

Conclusions

Ever since the Yule–Nielsen effect has been observed and described experimentally it has been recognized qualitatively that the magnitude of the effect is governed by the distance light scatters laterally in paper relative to the size of halftone dots. Excellent theoretical studies, such as those by Ruckdeschel and Hauser[6] and more recently by Kruse and Wedin,[7] have described two- and three-dimensional derivations of the Yule–Nielsen effect. Numerical simulations based on such theoretical models illustrate the significance of light scattering in halftone systems. However, they do not provide an easily used tool for estimating the magnitude of the Yule–Nielsen effect from direct measurements of the paper MTF constant, k_p. By combining theoretical with empirical models, practical relationships may be developed. Equation 24 is an example that suggests a simple but useful link between the halftone frequency, ω_o, lateral scattering, k_p, and the magnitude of the Yule–Nielsen effect. To achieve this link, we define the magnitude of the Yule–Nielsen effect, ΔR, as the difference between the reflectance predicted by the Murray–Davies model (Eq. 1 with $R_i = R_{\text{ink}}$ and $R_p = R_g$) and the reflectance observed experimentally for a halftone at $F_i = 0.5$:

$$\Delta R = (\text{Murray–Davies reflectance}) - (\text{experimental reflectance}). \tag{25}$$

The maximum value of ΔR is predicted to be the difference between the Murray–Davies reflectance and the Yule–Nielsen reflectance at $n = 2$:

$$\Delta R_{\max} = (\text{Murray–Davies reflectance}) - (\text{Yule–Nielsen at } n = 2). \tag{26}$$

Then the Yule–Nielsen effect may be defined as follows:

$$\text{Yule–Nielsen effect} = \Delta R / \Delta R_{\max}. \tag{27}$$

The relationship between the Yule–Nielsen effect defined by Eq. 27 and the value of the MTF_p constant, k_p, may be modeled easily and quickly by applying, in sequence, Eqs. 24, 4, 3, and then Eq. 1 with $R_i = R_i(F_i)$ and $R_p = R_p(F_p)$. If we assume that the dot edge effect is negligible ($k_i = 0$, or $v = 0$), then the Yule-Nielsen effect varies with the product $k_p\omega_o$ as shown in Fig. 9.

Among researchers and graphic arts professionals known to the authors it is popularly believed and observed that the shape of the halftone dot will have an effect on the Yule–Nielson effect. Figure 9 and Eq. 24 apply strictly only to one-dimensional halftone lines. If one were to develop an a priori model to describe halftone dots of other shapes, then a much more involved two-dimensional Fourier analysis, such as that described by Ruckdeschel and Hauser[6] and more recently by Kruse and Wedin,[7] would be required. However, one might expect, empirically, that Eq. 24 would apply as a reasonably close approximation to the behavior of other types of halftone systems provided appropriate values for the exponential constant, A, are chosen. If this is the case, then one might be able to make direct measurements of the empirical w constant, as described previously,[15]

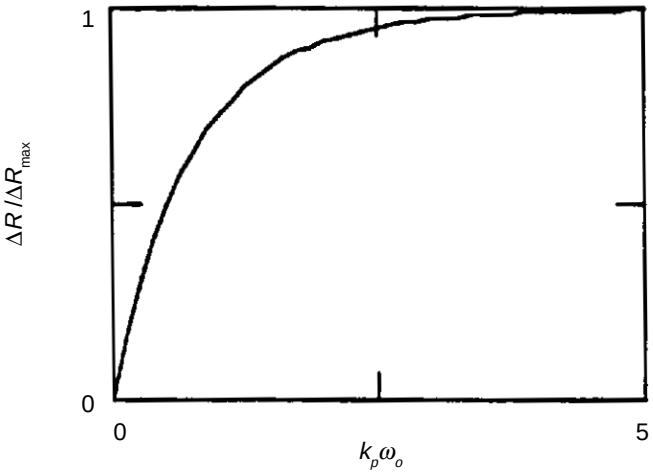

Figure 9. The magnitude of the Yule-Nielsen effect, $\Delta R / \Delta R_{max}$, as a function of the product $k_p \omega_o$.

and plot the results against the known values of the product, $k_p \omega_o$. Then by fitting the data to Eq. 24 a value of the constant A would perhaps provide a direct experimental characterization of the magnitude of the effect of dot shape, the effect of ink penetration, or other effects on the magnitude of the Yule–Nielsen phenomenon. The thrust of work currently under way in the authors' laboratories is focused on examining the utility of these semiempirical models for characterizing such effects.

Acknowledgment. This work was supported by grants from Mead Central Research and 3M Corporation. Special thanks to Bruce Blom, Andrew Virth, and Dick Fisch.

Appendix: Printing and Measuring Halftones

To compare theory with printed halftones, a set of straight-line halftone gray scales, ranging $0 \le F_i \le 1$, were prepared at line frequencies, ω_o, ranging from 2.4 to 7.7 line pairs per millimeter (60 to 195 lpi). These patterns were printed with an offset lithographic press, using a conventional aluminum printing plate prepared by the School of Printing at Rochester Institute of Technology. The plate was prepared from a photographic film, using conventional techniques. Once the halftone gray scales were printed, they were examined under a microscope with a field of view of 4.0 mm. The microscope image was captured with a CCD camera and frame grabber, which digitized the image at 464 by 512 pixels as described previously.[15] Pixel values captured in this way were corrected for a background "dark signal" by subtracting the pixel value obtained by capturing an image with the lens cap in place. The resulting pixel values in the image were then ratioed, pixel by pixel, against a similarly corrected reference white, and the result was multiplied by the known reflectance of the reference. The result was a 464 by 512 array of reflectance values representing the image observed through the microscope. From this reflectance matrix, a histogram of reflectance values was determined. Figure 3 illustrates such a histogram for a 60-lpi halftone nominally printed at $F_i = 0.50$. The reflectance values at the peaks corresponding to the ink, R_i, and the paper, R_p, are easily measured from the histogram. In addition, an experimental value of F_i can be measured as the relative areas under the histogram curves with the threshold reflectance between dot and paper defined as the saddle point between the peaks in the histogram.

Nomenclature

F_i	=	dot area fraction
F_p	=	paper area fraction, $F_p = 1 - F_i$
R_i	=	reflectance of the halftone ink dot, assumed to be a constant in Eqs. 1 and 2
R_p	=	reflectance of the paper between the dots, assumed to be a constant in Eqs. 1 and 2
R_g	=	intrinsic reflectance of the paper at $F_i = 0$
R_{ink}	=	reflectance of the ink on paper at $F_i = 1.00$
T_i	=	transmittance of the ink layer of the dot at $F_i = 1$, equal to $(R_{\text{ink}}/R_g)^{1/2}$
$R_p(F_p)$	=	mean value of reflectance of paper between halftone dots, measured experimentally from a peak in the histogram distribution of reflectance, and observed to be a function of the dot area fraction, F_i
$R_i(F_i)$	=	mean value of halftone ink dot, measured experimentally from a peak in the histogram distribution of reflectance and observed to be a function of the dot area fraction, F_i
$H(R)$	=	relative frequency of occurrence of a given R in a histogram
R_t	=	reflectance at the boundary between ink dot and paper, and used to threshold between ink and paper

References

1. A. Murray, *J. Franklin Inst.* **221**: 721 (1936).
2. J. A. S. Viggiano, *TAGA Proc.* p. 647 (1985).
3. J. A. Yule and W. J. Nielsen, *TAGA Proc.* p. 65 (1951).
4. J. S. Harrington, *TAGA Proc.* p. 144 (1991).
5. Y. Shiraiwa and T. Mizuno, *J. Imaging Sci. Technol.* **37**: 385 (1993).
6. F. Ruckdeschel and O. G. Hauser, *Appl. Opt.* **17**: 3376 (1978).
7. B. Kruse, and Mikael Wedin, Modeling of dot gain in halftone color prints, *MS Dissertation*, Department of Electrical Engineering, Linkoping University, Sweden, 1995.
8. W.W. Pope, *TAGA Proc.* p. 142 (1989).
9. F. R. Clapper and J. A. Yule, *J. Opt. Soc. Am.* **43**: 600 (1953).
10. F. P. Callahan, *J. Opt. Soc. Am.* **42**: 104 (1952).
11. J. A. C. Yule, D. J. Howe, and J. H. Altman, *TAPPI* **50**: 337 (1967).
12. J. R. Huntsman, *J. Imaging Technol.* **13**: 136 (1987).
13. M. Pearson, *TAGA Proc.* p. 415 (1980).
14. Peter G. Engeldrum, *J. Imaging Sci. Technol.* **38**: 545 (1994).
15. J. S. Arney, P. G. Engeldrum, and H. Zeng, An expanded Murray-Davies model of tone reproduction in halftone imaging, *J. Imaging Sci. Technol.* **39**: 502 (1995).
16. J. S. Arney, C. D. Arney, M. Katsube, and P. G. Engeldrum, An MTF analysis of paper, *J. Imaging Sci. Technol.* **40**: 19 (1996).
17. P. G. Engeldrum and B. Pridham, *TAGA Proc.* (1995).
18. P. Oittinen, in *Advances in Printing Science & Technology*, W. H. Banks, Ed., **16**: 121 (1982).
19. J. L. Kofender, Optical spread functions and noise characteristics of selected paper substrates measured in typical reflection optical system configurations, *Master's Thesis,* Center for Imaging Science, Rochester Institute of Technology, New York (1987).
20. M. Maltz, *J. Appl. Photogr. Eng.* **9**: 83 (1983).
21. J. S. Arney and P. G. Engeldrum, An optical model of tone reproduction in hard copy halftones, *Proceedings of IS&T's 11th International Congress on Advances in Non-Impact Printing,* Hilton Head, SC, Oct. 29-Nov. 3,1995.